Graphene-protected Fe layers atop Ni(111): Evidence for strong Fe-graphene interaction and structural bistability

E. A. Soares,[1,*] G. J. P. Abreu,[1,2] S. S. Carara,[1,3] R. Paniago,[1] V. E. de Carvalho,[1] and H. Chacham[1]

[1]*Departamento de Física, ICEx, Universidade Federal de Minas Gerais, Belo Horizonte, MG, Brazil*

[2]*Department of Physics, Penn State University, University Park, Pennsylvania 16802, USA*

[3]*Instituto de Física, Universidade Federal de Mato Grosso, Cuiabá, MT, Brasil*

(Received 6 February 2013; revised manuscript received 10 September 2013; published 14 October 2013)

The intercalation of different metals underneath the graphene sheet has opened the possibility of preparing new low-dimensional structures that could present quantum-size effects. Knowing the surface crystallograpy of these low-dimensional systems is mandatory for a complete understanding of their physical and chemical properties. In this work, we present a combined low-energy electron diffraction (LEED), x-ray photoelectron spectroscopy, and first-principles calculations study of the structural properties of graphene-protected Fe films on Ni(111). The results indicate that graphene interacts strongly with the topmost Fe atoms, similar to graphene on Ni(111). For one and two Fe monolayer films, the Fe is isostructurally deposited on Ni (fcc on fcc), and graphene is deposited commensurably with the underlying Fe surface atoms. For one Fe monolayer case, the LEED data indicate the coexistence of two types of crystalline domains, named top-fcc and bridge-top structures. Our first-principles calculations show that for the graphene/Fe/Ni system, the total energies of the the top-fcc and bridge-top structures are nearly degenerate, consistent with the observed bistability.

DOI: 10.1103/PhysRevB.88.165410 PACS number(s): 68.35.B−, 61.48.Gh

I. INTRODUCTION

Graphene layers grown on metal surfaces, especially of the noble and transition metals, have been motivating several works aiming at understanding their properties with respect to the surface protection as well as the metal film intercalation underneath the graphene. It has been demonstrated, both by experiments and by calculations, that graphene films grown on metallic substrates have the ability of protecting the surface from corrosion processes involving reactions with the environment. This protection from oxidation has been observed experimentally for graphene on Cu, Ni, and Cu/Ni alloys,[1–4] for Ru films on graphene-covered fused silica substrates,[5] and predicted by first-principles calculations for Al(111),[6] Co(111), Ni(111), and Cu(111).[7] A molecular dynamics calculation has shown that the strong O_2 binding energy in the gas phase of 6.7 eV is reduced to 1.8 eV when the molecule is on graphene and also that hydrogen-passivated Si and Fe atoms incorporated in graphene repel O_2 molecules.[8] This improved resistance to oxidation is potentially important, especially for applications in catalysis since it is known that many metals can not be used as catalysts because, in their oxidized state, they present no or very poor catalytic activity. Although the amount of investigation on this subject is yet small, it has been argued that inert graphene layer deposited on metal surfaces can be transformed to a very active catalyst by embedding metal clusters and individual atoms in defects in graphene.[8] Furthermore, the deposition of metal atoms on a graphene-covered metallic surface can form clusters on the graphene layer, be incorporated to the graphene defects, or diffuse through the graphene to form metallic layers in-between the graphene and the substrate. This last process has been called metal incorporation in the graphene-metal interface. It has been observed that the intercalation process can result in quasi-free-standing graphene exhibiting high quality comparable to that mechanically cleaved, that is, low sheet resistance, optical transparency, large electron mobility at room temperature, the half-integer quantum Hall effect, and high thermal conductivity, aside from presenting, in some systems, a zero-band gap at the Dirac point.[9–11] By this way, graphene layers of high quality and of different thicknesses have been prepared and transferred to another material for applications.

Beyond other new important properties that may be discovered, it is expected that by intercalating metals underneath the graphene layer it will be possible to decouple the graphene from the metal surface. According to literature, investigations have been performed mainly on three surfaces Ni(111), Ir(111), and Ru(0001), but with different adsorbed atoms: Fe, Cu, Ag, Au, Al, Na, K, and Cs on graphene/Ni(111); Pt, W, Re, Fe, and Au on graphene/Ir(111); and Pt, Pd, Ni, Co, Au, In, and Ce on graphene/Ru(0001).[10–12] These studies have revealed that there are important differences in the electronic behavior of such systems (for example, the opening up of the Dirac point band gap) as well as in the sites occupied by the adsorbed atom in the interface structure. For example, the intercalation of Pt, Pd, Ni, or Co on Ru(0001) preserves the size of the Moiré patterns whereas for Au, In, or Ce the periodicity of the Moiré pattern is modified.[12]

The intercalation, in the monolayer regime, of different metals such as Au,[13] Ag,[14] Cu,[15,16] Fe,[17–19] Sn, and Al[20,21] underneath a graphene sheet grown on Ni(111) has been extensively studied in the last years. These intercalated systems are interesting because their electronic structure and physical properties are similar to bulk classical graphite intercalation compounds. The possibility of preparing structures which can not be obtained in bulk graphite is also very attractive. Since they are low-dimensional systems, they could exhibit quantum-size effects such as oscillations of the valence band electron density near the Fermi level with respect to the thickness of the intercalated layers.

It has been shown by photoemission spectroscopy and first-principles calculations[17–19] that, after annealing of 1 and 2 Fe monolayers deposited over graphene on Ni(111), there is an intercalation of the Fe film underneath the graphene layer leading to the formation of graphene-protected fcc Fe films on Ni(111) where the Fe layers follow the fcc stacking of the substrate and the graphene has the same registry as for the Ni(111). However, the structural properties of the graphene-protected Fe films on Ni(111) still remain unexplored by techniques more sensitive to the surface structures.

In this paper, we present a combined low-energy electron diffraction (LEED), x-ray pholotelectron spectroscopy (XPS), and density-functional-theory- (DFT-) based first-principles calculations study of the structural properties of Fe monolayers intercalated underneath a graphene sheet epitaxially grown on Ni(111).

II. EXPERIMENTAL AND THEORETICAL DETAILS

The experiments have been carried out in a VG Escalab ultrahigh-vacuum (UHV) system with a base pressure of 1×10^{-10} mbar. The UHV system was equipped with the standard facilities for sample preparation (cleaning, heating, and deposition) and characterization (Auger, x-ray, and ultraviolet photoemission and Mössbauer spectroscopies) as well as with a computer-controlled four-grid LEED optics.

The Ni(111) single crystal, provided by Surface Preparation Laboratory,[22] was cleaned by cycles of sputtering (1-keV Ar^+ ions for 30 min) and annealing ($T = 700$ K for 20 min) until no contamination was detectable by x-ray photoelectron spectroscopy (XPS). The graphene was grown on Ni(111) by exposing the surface to an atmosphere of 2×10^{-6} mbar of C_3H_6 for 10 min at a temperature of (810 ± 30) K, as previously described in the literature.[16] High-purity Fe monolayers (from 1 up to 3) were evaporated using an omicron *e*-beam source onto the Ni(111) covered by graphene at room temperature. After Fe deposition, the surface was annealed at (590 ± 30) K for 15 min. The surface chemical composition was probed by XPS using both Al-K_α and Mg-K_α lines. The diffracted intensities as a function of electron energy (LEED-IV curve) were collected for all available beams at nominal normal incidence in the range of 50–400 eV, normalized by the incident electron current and smoothed using a three-point least-squares cubic polynomial algorithm. The symmetry-equivalent beams were then averaged. Before each Fe intercalation, the Ni(111) surface was cleaned and a new graphene layer was grown.

The LEED quantitative theoretical analysis was carried out using the method of symmetrized automated tensor LEED with the programs associated to calculate the scattering phase shifts, using the approximation of the muffin-tin potential.[23] The agreement between the experimental and theoretical LEED-IV curves was quantified by the *R* factor proposed by Pendry[24] (R_P). In all cases where mixed domains were considered, the calculated spectra were derived from incoherently summing over the different terraces. When mixing different domains on the surface, the number of fit parameters increases and, consequently, the R_P factor decreases. A modified Hamilton ratio[25,26] was used to verify if whether the improved fit actually implies a better structural solution. It has been empirically observed that the Hamilton ratio should exceed 3.0 to indicate real improvements, while values below 1.0 indicate merely a better fit due to additional parameters.

The *ab initio* calculations were performed using the SIESTA code.[27,28] The applied first-principles methodology is based on density-functional theory[29] as implemented in the SIESTA code. Norm-conserving pseudopotentials of Troullier-Martins[30] in Kleinman-Bylander nonlocal form were used to represent the ionic core potential. We make use of the generalized gradient approximation, as parametrized by the Perdew *et al.*[31] scheme, for the exchange-correlation functional. The Kohn-Sham orbitals[32] are expanded in a linear combination of numerical atomic orbitals of finite range which is determined by a common confinement energy shift of 0.01 Ry.[33] The fineness of the real-space grid integration is determined by a minimal energy cutoff of 200 Ry.[34] The valence electrons of the C, Ni, and Fe atoms were represented by a basis set consisting of double-zeta radial functions per angular momentum plus polarization functions (DZP). Tests were made to find the best basis set and calculation input parameters to reproduce the experimental values of bond lengths and lattice parameters of the Ni(111) surface. Our model for unit cell of the graphene/Fe/Ni(111) heterostructure is composed by 9 to 10 nickel atoms, 1 to 2 iron atoms, and 2 carbon atoms (graphene unit cell) in such a way that the total number of atoms of each system is always equal to 13. In both unit cells, the distance between the top layer and its periodic image is about 45 Å, which ensures that there is no interaction between successive periodic images along the *z* direction (which is the one perpendicular to the surface). The graphene/Fe/Ni(111) unit cell is periodic in the *x* and *y* directions. The respective Brillouin zone is sampled by a 15 $\times$ 15 $\times$ 2 Monkhorst-Pack grid.[35] The geometries were fully optimized until all the force components became smaller than 0.05 eV/Å.

III. RESULTS AND DISCUSSION

After growing graphene on the Ni(111)(1$\times$1) surface, we evaporated one, two, and three monolayers (ML) of Fe over it at room temperature. After deposition, the diffraction patterns from the surface exhibited the (1$\times$1) symmetry but with high background intensity. After annealing the sample for 15 min at 590 K, the LEED patterns became again well defined showing the (1$\times$1) symmetry with low background intensity (Fig. 1).

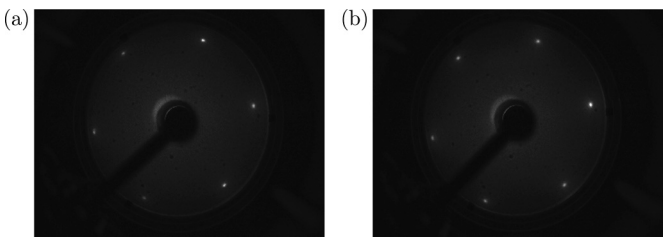

FIG. 1. LEED patterns at $E = 99$ eV for (a) C/1 ML Fe/Ni(111)(1$\times$1) and (b) C/2 ML Fe/Ni(111)(1$\times$1), both after annealing.

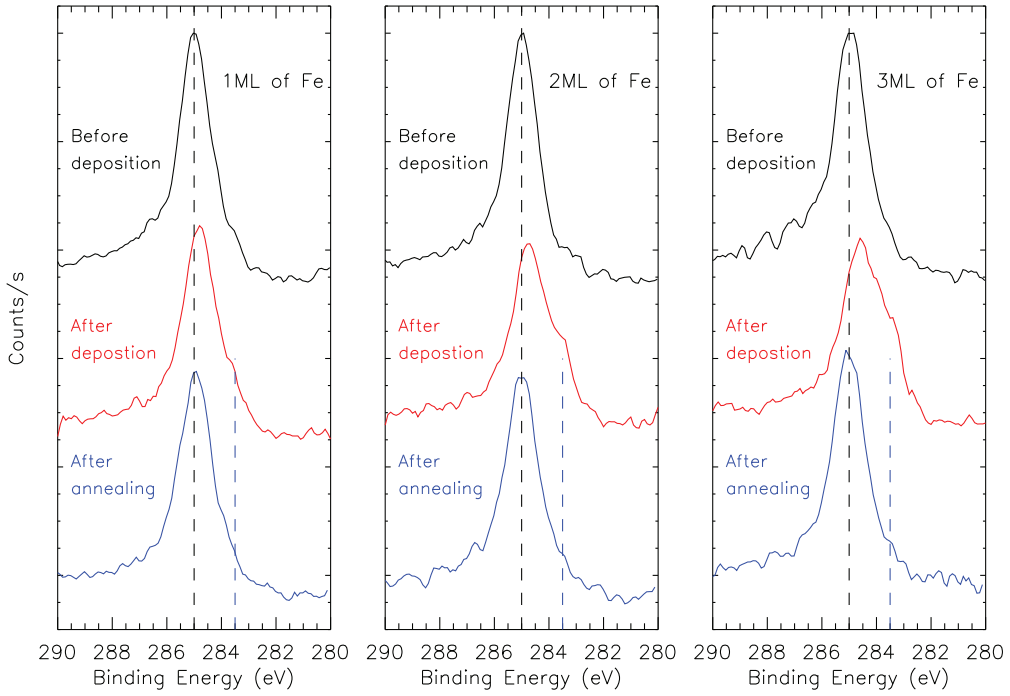

FIG. 2. (Color online) (a) C 1*s* photoemission spectra before (black) and after (red) deposition, and after (blue) the annealing procedure for 1, 2, and 3 ML of Fe.

XPS measurements showed the presence of metallic Fe with no trace of oxide formation. Figure 2 shows XPS data in the C 1*s* photoemission range before and after deposition, and after the annealing procedure for 1, 2, and 3 ML of Fe. The spectra were normalized with respect to the C 1*s* photoemission peak from the graphene on Ni(111) before deposition. We clearly see a decrease on the intensity of the C 1*s* peak after deposition. This intensity reduction originates from the fact that now the C 1*s* photoelectrons have to cross the deposited Fe layers reducing the number of electrons that reach the detector without being scattered. As the Fe thickness increases, a shoulder develops at binding energy of about 283.5 eV. We do not have a clear picture yet why this is happening. Based only on the binding energy of the C 1*s* peak shoulder, a possible explanation might be the formation of small islands of Fe_3C.[36,37]

After annealing, the C 1*s* intensity recovers its original value, demonstrating that the C 1*s* photoelectrons are not attenuated by the Fe layers anymore. This intensity recovering is a strong evidence that the Fe atoms are now under the graphene sheet. The shoulder disappears and the C 1*s* photoemission peak exhibits now only a single peak at binding

TABLE I. The final R_P factors for models having 1 ML of Fe between the graphene sheet and the Ni(111) surface after the structural and nonstructural parameters optimization. The two sets of lowercase letters correspond to the stacking of the carbon atoms in the unit cell with respect to the Fe layer. The uppercase letter in italic corresponds to the stacking of the Fe layer with respect to the topmost nickel layer labeled by the uppercase letter A.

Model	R_P factor
Models without stacking fault	
top-fcc *C*ABC	**(0.27 ± 0.05)**
top-hcp *C*ABC	(0.70 ± 0.14)
fcc-hcp *C*ABC	(0.68 ± 0.13)
bridge-top *C*ABC	**(0.35 ± 0.07)**
Models with stacking fault	
top-fcc *B*ABC	(0.83 ± 0.16)
top-hcp *B*ABC	(0.74 ± 0.15)
hcp-fcc *B*ABC	(0.71 ± 0.14)
bridge-top *B*ABC	(0.79 ± 0.16)
Models with domain mixing	
60% *top-fcc* + 40% *bridge-top*	(0.20 ± 0.04)

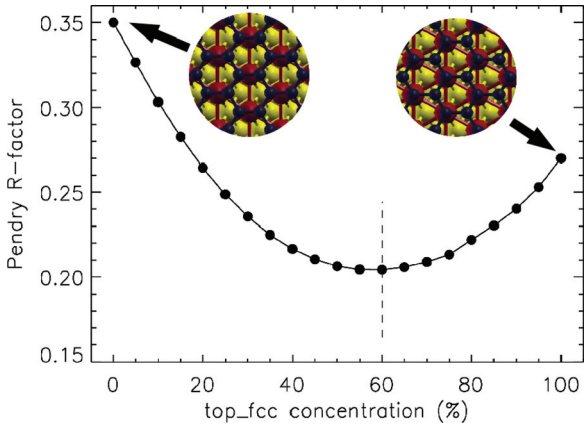

FIG. 3. (Color online) The Pendry R_P factor for surface models having a mixture of top-fcc and bridge-top domains for the C/1 ML Fe/Ni(111)(1×) system. On the left (0%), the surface contains only bridge-top domains. On the right (100%), the surface is completely covered by top-fcc domains. In-between, the surface is a mixture of the two models.

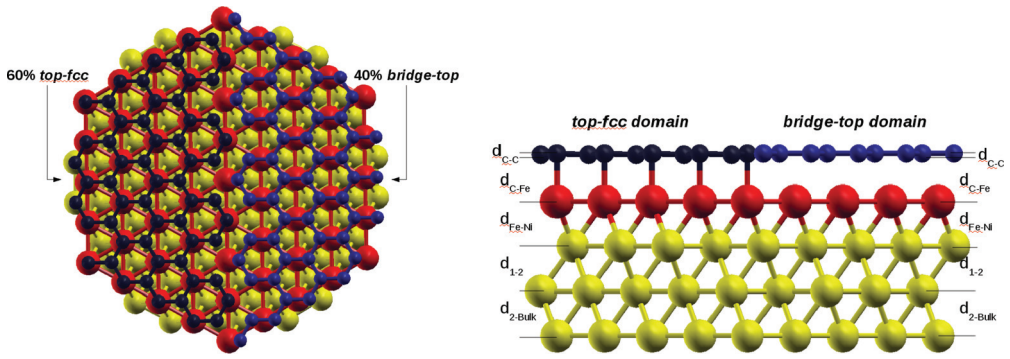

FIG. 4. (Color online) Top and side views of the structural model having the coexistence of top-fcc and bridge-top domains that best fit the experimental LEED-IV curves after intercalation of 1 ML of Fe.

energy of 285.0 eV. This binding energy is exactly the same value observed for the C 1*s* photoemission peak after the graphene growth on Ni(111), suggesting that the graphene is strongly coupled to the Fe layers.[38]

The LEED patterns were then collected for 1 and 2 ML of Fe after intercalation and the LEED-IV curves were extracted from the digitized patterns. After averaging of the symmetrically equivalent beams, the experimental beams were reduced to 5 and 3 nonequivalent beams defining a total energy range of 1025 and 700 eV for the 1 and 2 ML of Fe, respectively. Several different structural models, including different Fe thickness, stacking faults in the Fe layers with respect to the substrate underneath, and having Fe layers above and below the graphene sheet were considered in the LEED analysis. All models where the Fe monolayers were over the graphene sheet resulted in R_P factors higher than 0.8 and were not considered for further optimizations. The very poor agreement between the models having Fe layers over the graphene sheet and the experimental LEED-IV curves supports our model with Fe intercalated between the graphene and Ni(111) surface. In the next two sections, we discuss in details the structural analysis of the 1- and 2-ML Fe films after intercalation.

A. C/1 ML Fe/Ni(111)(1 × 1) structural analysis

As expected, structural models having 2, 3, and 4 Fe monolayers did not fit the experimental data for the 1-ML Fe film and produced unreasonable results and unrealistic structures characterized by R_P values higher than 1.0. The Pendry's R factor for all possible models having 1 Fe layer underneath graphene is presented in Table I. Models with stacking faults also did not show a good agreement with the experimental data as demonstrated by very high values of R_P. The best experiment-theory agreement was obtained by having the Fe layer following the fcc stacking of the substrate and the carbon atoms in the top and fcc hollow sites. However, the bridge-top model can not be ruled out because the difference between the R_P of the two models is within the error bars. This small difference may be an indication that, in our experiment, both structures may be present on the surface. In our DFT investigation, we found that the energy of the top-fcc model is 0.1 eV per unit cell smaller than the energy of the bridge-top model. Therefore, if the two structures coexist on the surface, domains with Fe layers arranged by the top-fcc model should be more favorable than bridge-top domains. In order to carefully investigate this point, we have allowed the coexistence of top-fcc and bridge-top domains on the surface in the LEED calculations.

Figure 3 shows the R_P as a function of the top-fcc domain coverage on the surface. By mixing the bridge-top and the top-fcc models, a well-defined minimum is observed. For a model consisting of 60% of top-fcc and 40% of bridge-top domains, the lowest $R_P = (0.20 \pm 0.04)$ is achieved. By applying the Hamilton test to this model, we get a ratio of $H = 4.35$, indicating a real improvement of the structural model. Figure 4 shows a schematic drawing of this structural model.

In Table II, we present the vertical distances obtained from the LEED analysis for both domains and from our

TABLE II. The structural and nonstructural parameters of the *top-fcc* and *bridge-top* domains obtained from LEED structural determination and from our DFT calculations for the C/1 ML Fe/Ni(111)(1×1) system. Θ_D^{C} and $\Theta_D^{\mathrm{Ni_{surf}}}$ are the Debye temperatures of the graphene and the topmost Ni layers, respectively. Vo_i is the imaginary part of the inner potential.

	Top-fcc domain	*Top-fcc* (DFT)	*Bridge-top* domain	*Bridge-top* (DFT)
$d_{\mathrm{C\text{-}C}}$ (Å)	0.08 ± 0.05	0.03	0.10 ± 0.05	0.01
$d_{\mathrm{C\text{-}Fe}}$ (Å)	2.06 ± 0.04	2.12	2.02 ± 0.04	2.15
$d_{\mathrm{Fe\text{-}Ni}}$ (Å)	2.06 ± 0.07	2.05	2.04 ± 0.07	2.05
d_{12} (Å)	2.03 ± 0.06	2.04	2.02 ± 0.06	2.05
$d_{\mathrm{2\text{-}Bulk}}$ (Å)	2.03 ± 0.06	2.03	2.04 ± 0.06	2.04
Θ_D^{C} (K)	600 ± 80		600 ± 80	
$\Theta_D^{\mathrm{Ni_{surf}}}$ (K)	350 ± 80		350 ± 80	
Vo_i (eV)	-5.0		-5.0	

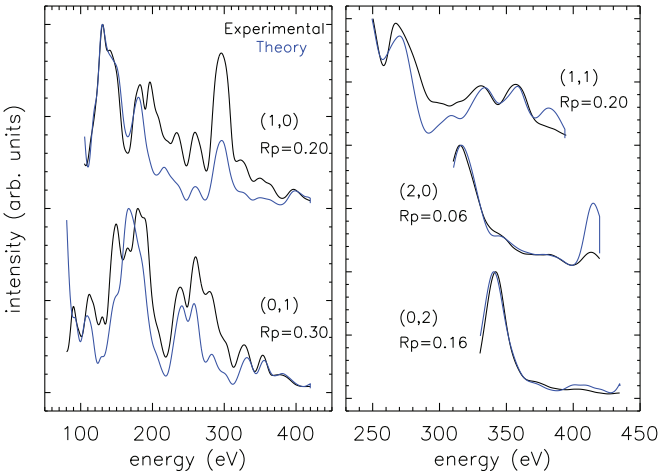

FIG. 5. (Color online) The experimental (black lines) and the best theoretical (blue lines) LEED-IV curves for the C/1 ML Fe/Ni(111)(1×1) system.

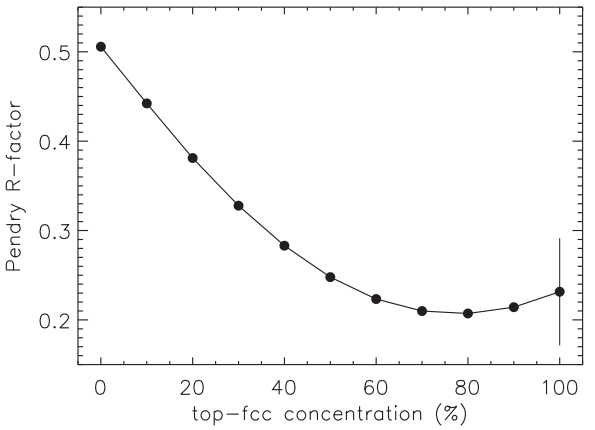

FIG. 6. The Pendry R_P factor for surface models having a mixture of top-fcc and bridge-top domains for the C/2 ML Fe/Ni(111)(1×1) system. On the left (0%), the surface contains only bridge-top domains. On the right (100%), the surface is completely covered by top-fcc domains. In-between, the surface is a mixture of the two models.

DFT calculations for the top-fcc and bridge-top models. It is clear that the structural parameters of both domains are essentially the same as well as for both models predicted by our theoretical simulations. Although atomic displacements parallel to the surface are allowed for the bridge-top model due to its lower symmetry, no significant deviations from the starting structure (the C-C atom bond center point being on top of the first-layer Ni atom) were observed after optimization. It is also worth to point out that the two models are related by a registry shift of the graphene sheet. Table II also shows that our experimental and theoretical results are consistent. The comparison between the experimental and the theoretical LEED-IV curves corresponding to the best mixed-termination model is presented in Fig. 5. We clearly see that most of the diffracted peaks are well reproduced in the theoretical LEED-IV curves. FeNi alloy formation on the interface was also tested using the average T-matrix approximation (ATA).[39,40] All alloy models considered have higher R_P factors than the top-fcc single-domain model. However, Fe and Ni atoms scatter electrons very similarly and the ATA was not too sensitive to changes in the alloy concentration.

It is worth to point out that, from our experiment, we can not conclude whether the coexistence of both structures was already present on the surface after the graphene growth on Ni(111) or if it was induced by the Fe intercalation. The reason for that is that we did not perform a full LEED structural analysis of the graphene/Ni(111) surface used for the 1-ML Fe intercalation.

TABLE III. The final R_P factors for models having 2 ML of Fe between the graphene sheet and the Ni(111) surface after the structural and nonstructural parameters optimization. The two sets of lowercase letters correspond to the stacking of the carbon atoms in the unit cell with respect to the topmost Fe layer. The two uppercase letters in italic correspond to the stacking of the iron layers with respect to the topmost nickel layer labeled by the first uppercase letter A from right to left.

Model	R_P factor
Models without stacking fault	
*top-fcc BC*ABC	**(0.23 ± 0.06)**
*top-hcp BC*ABC	(0.54 ± 0.14)
*fcc-hcp BC*ABC	(0.53 ± 0.14)
*bridge-top BC*ABC	(0.51 ± 0.13)
Models with stacking fault	
*top-fcc AC*ABC	(0.58 ± 0.15)
*top-hcp AC*ABC	(0.54 ± 0.14)
*hcp-fcc AC*ABC	(0.59 ± 0.15)
*bridge-top AC*ABC	(0.60 ± 0.16)
*top-fcc CB*ABC	(0.61 ± 0.16)
*top-hcp CB*ABC	(0.58 ± 0.15)
*hcp-fcc CB*ABC	(0.57 ± 0.15)
*bridge-top CB*ABC	(0.60 ± 0.16)
*top-fcc AB*ABC	(0.57 ± 0.15)
*top-hcp AB*ABC	(0.49 ± 0.13)
*hcp-fcc AB*ABC	(0.55 ± 0.15)
*bridge-top AB*ABC	(0.59 ± 0.15)

B. C/2 ML Fe/Ni(111)(1 × 1) structural analysis

Similarly to the 1-ML Fe thick film case, we investigated the possibility of having intercalated an amount of Fe different from 2 ML on graphene grown on Ni(111) by considering

TABLE IV. The structural parameters corresponding to the best model from LEED structural determination and from our DFT calculations for C/2 ML Fe/Ni(111)(1×1).

	top-fcc (LEED)	*top-fcc* (DFT)
$d_{\text{C-C}}$ (Å)	0.04 ± 0.05	0.03
$d_{\text{C-Fe}}$ (Å)	2.14 ± 0.04	2.08
$d_{\text{Fe-Fe}}$ (Å)	1.97 ± 0.06	2.11
$d_{\text{Fe-Ni}}$ (Å)	2.13 ± 0.07	2.04
d_{12} (Å)	2.03 ± 0.06	2.06
$d_{\text{2-Bulk}}$ (Å)	2.03 ± 0.06	2.03
Θ_D^{C} (K)	600 ± 100	
$\Theta_D^{\text{Ni}_{\text{surf}}}$ (K)	300 ± 100	
Vo_i (eV)	−7.0	

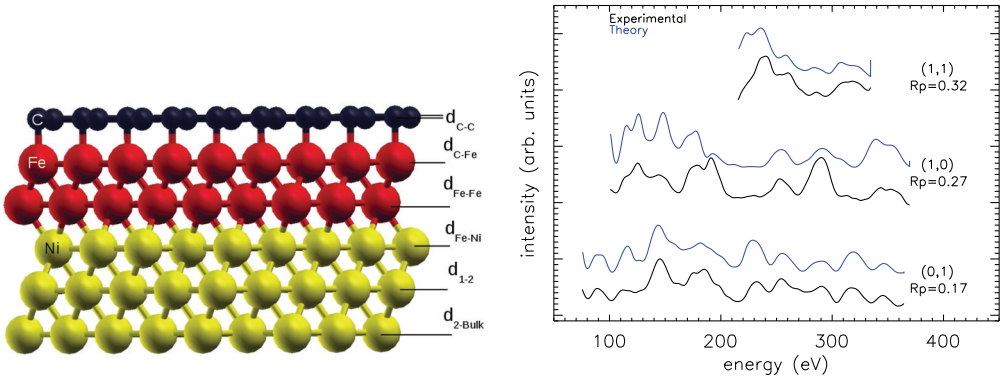

FIG. 7. (Color online) Top panel: side view of the best top-fcc model obtained from the LEED analysis after the intercalation of 2 ML of Fe. Bottom panel: experimental (black lines) and theoretical (blue lines) LEED-IV curves evaluated for the best model.

models with different Fe coverages. As expected, structural models having 1, 3, and 4 Fe layers did not fit the experimental data for the 2-ML Fe film and produced unrealistic structures characterized by R_P values higher than 0.8.

In Table III, the Pendry's R factor for all possible models having 2 Fe layers underneath graphene is presented. Models with stacking faults also did not show a good agreement with the experimental data as demonstrated by very high values of R_P. The best experiment-theory agreement was obtained by having the 2 Fe layers following the fcc stacking of the substrate and the carbon atoms in the top and fcc hollow sites. The good agreement between experiment and theory is reflected by a final R_P value of (0.23 ± 0.06).

Now, the bridge-top model did not fit our experimental data for the 2-ML Fe thick film exhibiting a $R_P = 0.51$, suggesting that the coexistence of top-fcc and bridge-top domains on the surface is unlikely for this growth. Again, in order to carefully investigate this point we have allowed the coexistence of top-fcc and bridge-top domains on the surface in the LEED calculations. The R_P as a function of the top-fcc domain coverage on the surface can be seen in Fig. 6.

For a model consisting of 80% of top-fcc and 20% of bridge-top domains the lowest $R_P = (0.21 \pm 0.06)$ is achieved. By applying the Hamilton test to this model, we get a very low value for the Hamilton ratio of $H = 0.26$ indicating no real improvement of the structural model. This result is also predicted by our DFT calculations. After the total energy minimization, the final atomic geometry obtained moved from the 2-ML Fe bridge-top model to the top-fcc model, suggesting that this last structure is the most favorable.

The final structural parameters corresponding to the best top-fcc model obtained from the LEED analysis and the DFT total energy minimization are presented in Table IV. A side view of this model is shown on the top panel of Fig. 7. The structure is similar to the one obtained for C/1 ML Fe/Ni(111)(1×1). The main observed structural features are a small rumple of (0.04 ± 0.05) Å between the two carbon atoms in the graphene unit cell, a contraction in distance between the Fe layers and an expansion of the interlayer distance at the Fe-Ni interface, when compared to the bulk interlayer distances of the Ni(111) (2.03 Å) or fcc-Fe(111) (2.07 Å), respectively. The comparison between the experimental and theoretical LEED-IV curves calculated for the best-fit model described in Table IV are presented on the bottom panel of Fig. 7. We clearly see that all the main diffracted peaks presented in the experimental LEED-IV curves are reproduced in the theoretical ones.

IV. CONCLUSION

In summary, we have investigated by low-energy electron diffraction and first-principles calculations the structure of Fe layers intercalated between the graphene and the Ni(111) surface. From the intercalation experiments, we can conclude, based on the XPS data, that the graphene strongly interacts with the topmost Fe atoms since the C 1s binding energy is the same as for the graphene on Ni(111) (285.0 eV). This is consistent with the small C-Fe distances (between 2.0 and 2.1 Å) obtained from both the LEED structural determination and from our DFT calculations At least for the intercalation of 1 and 2 ML of Fe, the Fe layers follow the fcc stacking of the Ni(111) substrate. The coexistence of the top-fcc and bridge-top structures was observed for the intercalation of 1 ML of Fe. However, we can not conclude if the coexistence was already present on the surface after the growth of graphene on Ni(111) or it was induced by the Fe intercalation.

ACKNOWLEDGMENT

We would like to thank the Brazilian funding agencies CNPq, FAPEMIG, and CAPES, and the project "INCT de Nanoestruturas de Carbono" for financial support.

*Corresponding author: edmar@fisica.ufmg.br

[1]Y. S. Dedkov, M. Fonin, U. Rudiger, and C. Laubschat, Appl. Phys. Lett. **92**, 052506 (2008).

[2]S. Chen, L. Brown, M. Levendorf, W. Cai, S.-Y. Ju, J. Edgeworth, X. Li, C. Magnuson, A. Velamakanni, R. Piner, J. Kang, J. Park, and R. Ruoff, ACS Nano **5**, 1321 (2011).

[3]D. Prasai, J. C. Tuberquia, R. R. Harl, G. K. Jennings, and K. I. Bolotin, ACS Nano **6**, 1102 (2012).

[4]N. Kirkland, T. Schiller, N. Medhekar, and N. Birbilis, Corros. Sci. **56**, 1 (2012).

[5]E. Sutter, P. Albrecht, F. E. Camino, and P. Sutter, Carbon **48**, 4414 (2010).

[6]M. Topsakal, H. Sahin, and S. Ciraci, Phys. Rev. B **85**, 155445 (2012).
[7]J. Gao, J. Zhao, and F. Ding, J. Am. Chem. Soc. **134**, 6204 (2012).
[8]M. F. Chisholm, G. Duscher, and W. Windl, Nano Lett. **12**, 4651 (2012).
[9]F. Molitor, J. Guttinger, C. Stampfer, S. Droscher, A. Jacobsen, T. Ihn, and K. Ensslin, J. Phys.: Condens. Matter **23**, 243201 (2011).
[10]J. Wintterlin and M. L. Bocquet, Surf. Sci. **603**, 1841 (2009).
[11]E. Voloshina and Y. Dedkov, Phys. Chem. Chem. Phys. **14**, 13502 (2012).
[12]L. Huang, Y. Pan, L. Pan, M. Gao, W. Xu, Y. Que, H. Zhou, Y. Wang, S. Du, and H.-J. Gao, Appl. Phys. Lett. **99**, 163107 (2011).
[13]A. M. Shikin, G. V. Prudnikova, V. K. Adamchuk, F. Moresco, and K.-H. Rieder, Phys. Rev. B **62**, 13202 (2000).
[14]D. Farias, A. M. Shikin, K.-H. Rieder, and Y. S. Dedkov, J. Phys.: Condens. Matter **11**, 8453 (1999).
[15]A. M. Shikin, D. Farias, and K.-H. Rieder, Europhys. Lett. **44**, 44 (1998).
[16]Y. S. Dedkov, A. M. Shikin, V. K. Adamchuk, S. L. Molodtsov, C. Laubschat, A. Bauer, and G. Kaindl, Phys. Rev. B **64**, 035405 (2001).
[17]Y. S. Dedkov, M. Fonin, U. Rudiger, and C. Laubschat, Appl. Phys. Lett. **93**, 022509 (2008).
[18]X. Sun, A. Pratt, and Y. Yamauchi, J. Phys. D: Appl. Phys. **43**, 385002 (2010).
[19]M. Weser, E. N. Voloshina, K. Horn, and Y. S. Dedkov, Phys. Chem. Chem. Phys. **13**, 7534 (2011).
[20]E. N. Voloshina, A. Generalov, M. Weser, S. Böttcher, K. Horn, and Y. S. Dedkov, New J. Phys. **13**, 113028 (2011).
[21]A. D. Rafik Addou and M. Batzill, Surf. Sci. **606**, 1108 (2012).
[22]René Koper, http://www.surface-prep-lab.com.
[23]Barbieri/Van Hove SATLEED and Phase Shift package, http://www.ap.cityu.edu.hk/personal-website/Van-Hove_files/leed/leedpack.html.
[24]J. B. Pendry, J. Phys. C: Solid State Phys. **13**, 937 (1980).
[25]C. F. Walters, K. F. McCarty, E. A. Soares, and M. A. V. Hove, Surf. Sci. **464**, L732 (2000).
[26]E. A. Soares, M. A. Van Hove, C. F. Walters, and K. F. McCarty, Phys. Rev. B **65**, 195405 (2002).
[27]J. M. Soler, E. Artacho, J. D. Gale, A. García, J. Junquera, P. Ordejón, and D. Sánchez-Portal, J. Phys.: Condens. Matter **14**, 2745 (2002).
[28]E. Artacho, E. Anglada, O. Dieguez, J. D. Gale, A. García, J. Junquera, R. M. Martin, P. Ordejón, J. M. Pruneda, D. Sánchez-Portal, and J. M. Soler, J. Phys.: Condens. Matter **20**, 064208 (2008).
[29]P. Hohenberg and W. Kohn, Phys. Rev. **136**, B864 (1964).
[30]N. Troullier and J. L. Martins, Phys. Rev. B **43**, 1993 (1991).
[31]J. P. Perdew, K. Burke, and M. Ernzerhof, Phys. Rev. Lett. **77**, 3865 (1996).
[32]W. Kohn and L. J. Sham, Phys. Rev. **140**, A1133 (1965).
[33]J. Junquera, O. Paz, D. Sánchez-Portal, and E. Artacho, Phys. Rev. B **64**, 235111 (2001).
[34]J. Moreno and J. M. Soler, Phys. Rev. B **45**, 13891 (1992).
[35]H. J. Monkhorst and J. D. Pack, Phys. Rev. B **13**, 5188 (1976).
[36]S. J. Li, H. Yumonto, M. Shimotomai, and M. Ishihara, Thin Solid Films **345**, 23 (1999).
[37]H. Yumonto, Y. Nagamine, J. Nagahama, and M. Shimotomai, Vacuum **65**, 527 (2002).
[38]W. Zhao, S. M. Kozlov, O. Höfert, K. Gotterbarm, M. P. A. Lorenz, F. Viñes, C. Papp, A. Görling, and H.-P. Steinrück, New. J. Phys. **11**, 073050 (2009).
[39]J. Korringa, J. Phys. Chem. Solids **7**, 252 (1958).
[40]S. Crampin and P. J. Rous, Surf. Sci. **244**, L137 (1991).